International Journal of Mineral Processing 101 (2011) 28–36

Contents lists available at ScienceDirect

International Journal of Mineral Processing

journal homepage: www.elsevier.com/locate/ijminpro

Ore grade estimation by feature selection and voting using boundary detection in digital image analysis

Claudio A. Perez *, Pablo A. Estévez, Pablo A. Vera, Luis E. Castillo, Carlos M. Aravena, Daniel A. Schulz, Leonel E. Medina

Department of Electrical Engineering and Advanced Mining Technology Center, Universidad de Chile, Av. Tupper 2007, Santiago, Chile

ARTICLE INFO

Article history:
Received 28 February 2011
Accepted 10 July 2011
Available online 7 August 2011

Keywords:
Ore sorting
Rock lithological classification
Rock grindability
Rock image analysis

ABSTRACT

In mining, rock classification plays a crucial role at different stages of the extraction process ranging from the design of the mine to mineral grading and plant control. In this paper we present a new method to improve rock classification using digital image analysis, feature selection based on mutual information and a voting process to take into account boundary information. We extract rock color and texture features and using mutual information we selected 14 from 36 features to represent the data in a lower dimensional space. The original image was divided into sub-images that are assigned to one class based on the selected color and texture features using a set of classifiers in cascade. Additionally, using rock boundary information, a voting process for the sub-images within the same blob is performed. We compare our results based on sub-image classification to those obtained after the voting process and to those previously published on the same rock image database. We show that the RMSE on rock composition classification on a test database decreased 8.8% by using our proposed voting method with the automatic segmentation with respect to direct sub-image classification. The RMSE decreased 29.5% relative to previously published results with the same database using a mixture of dry and wet rock images. The RMSE decreased even more if we considered separately dry and wet rocks. Our proposed method could be implemented in real-time to estimate mineral composition and can be used for online ore sorting and/or classification.

1. Introduction

In mining, rock classification plays a crucial role at different stages of the extraction process ranging from the design of the mine to mineral grading and plant control (Chatterjee et al., 2010b). Characterization of the constituent rocks of an ore deposit including gangue material could be useful in the selection of the required equipment for excavation, and the strategies for blasting, among others. From a geological point of view, rock classification is useful for understanding the local properties of the ore deposit that determine the mine design.

Additionally, several processes in the mining plant can be optimized or improved by means of rock classification. For example, knowing rock types is important in determining various process parameters such as grindability, slurry viscosity, and screening efficiency, among others (Casali et al., 2001). In particular, lithological composition allows rock grindability characterization that in turn could be used to optimize mill operation. Consequently, an online ore composition estimation system that is able to detect ore hardness changes before the ore enters the mill can be used to control the mill speed improving the mill throughput processing (Tessier et al., 2007). Moreover, a mining plant could be optimized using ore sorting based on lithological composition to control the mill feeding.

Usually, rock classification or characterization is performed visually by mineralogists or geologists. However, a more sophisticated method for mineral identification for ore grading is done by collecting and chemically analyzing rock samples in a laboratory (Chatterjee et al., 2010b). Because of the time needed for the chemical analysis, it is not possible to perform it online. Therefore, a faster sensing system is desirable to achieve online estimation of rock composition. This could be possible with a machine vision system since visual classification of rocks is carried out by humans.

Machine vision in the mineral industry has been applied in several mining operations such as online inspection of crushed aggregates (Al-Batah et al., 2009), online ore sorting and classification (Casali et al., 2001; Chatterjee et al., 2010a, 2010b; Guyot et al., 2004; Perez et al., 1999; Singh and Rao, 2006; Tessier et al., 2007), particle and blast fragment size estimation and/or distribution (Al-Thyabat et al., 2007; Hunter et al., 1990; Koh et al., 2009; Petersen et al., 1998; Salinas et al., 2005; Thurley and Ng, 2008), and froth monitoring (for a complete review see Aldrich et al. (2010), and others).

In this study we focus on the rock classification problem. Early efforts to use machine vision in rock classification started in the 1990s.

* Corresponding author.
E-mail address: clperez@ing.uchile.cl (C.A. Perez).

0301-7516/$ – see front matter © 2011 Elsevier B.V. All rights reserved.
doi:10.1016/j.minpro.2011.07.008

Oestreich et al. (1995) utilized a color sensor system based on color vector angle to estimate the composition of a mixture of two minerals, chalcopyrite and molybdenite. Perez et al. (1999) and Casali et al. (2001) used a multi-layer neural network to classify seven classes of lithologies. They extracted color, texture and geometric features from the rock images and performed a feature selection using a genetic algorithm. The method included a rock segmentation scheme based on binarization and morphological operators. Singh and Rao (2006) studied ferruginous manganese ores with histogram analysis in the RGB color space, combined with textural analysis based on the gray level co-occurrence matrix and edge detection.

Tessier et al. (2007) presented a very complete study of an on-line automatic ore composition estimator mounted on a pilot plant. They studied five ore types from Raglan's mine in Canada and used principal component analysis (PCA) and wavelet texture analysis (WTA) for color and texture feature extraction, respectively. They obtained promising results in both dry and wet rock images. The studies presented by Chatterjee et al. (2010a, 2010b) analyzed minerals coming from two different deposits – limestone and iron – although very similar approaches were used in both cases. They selected a segmentation algorithm from several tests and then applied morphological, textural and color feature extraction. PCA was used to reduce the feature vector and a neural network was used for classification.

Other rock classification systems were reported by Paclik et al. (2005) who used local texture information with co-occurrence likelihoods to build an industrial rock classification system; Lepisto et al. (2005) applied Gabor filtering to different color spaces for the classification of natural rock images; Linek et al. (2007) combined Haralick features and wavelet analysis for classification of rocks in electrical borehole wall images which are used in the exploration of ocean basins and the ocean crust by drilling; Kachanubal and Udomhunsakul (2008) utilized a neural network combined with PCA and applied spatial frequency measurement to separate 26 stone classes; Donskoi et al. (2008) modeled and optimized a hydrocyclone using optical imaging and texture classification; Murtagh and Starck (2008) used up to fourth order moments of wavelet and curvelet transforms to classify images of mixture aggregate; Goncalves et al. (2009) presented a study for classification of macroscopic rock texture based on a hierarchical neuro-fuzzy model; and Singh et al. (2010) developed an application of image processing on basalt rock samples where parameters are input to a neural network for classification.

The main contribution of our study is the application of a method to extract and select features based on rock color and texture, and using rock boundary information to improve classification performance by a sub-image voting scheme. We compare our results to those previously published on the same database with significant reduction of error in estimating rock composition in digital images. Our proposed method could be implemented in real-time to estimate mineral composition and can be used for online ore sorting and/or classification.

2. Material and methods

Our proposed method for rock classification includes color and texture feature extraction and feature selection as well as use of a support vector machine (SVM) for classification. We also added a post-processing stage that includes rock segmentation based on the Watershed algorithm and a voting process based on this information enhances rock classification. Fig. 1 summarizes the main steps of the proposed method for image analysis.

2.1. Image segmentation

Several alternatives are available for partitioning a digital image into fragments with only one rock type. As in Tessier et al. (2007), we divided each digital image of 1024×1376 pixels into 512 sub-images of 64×43 pixels. These sub-images are of 1.5 cm^2 and have enough size to capture the relevant textural features (Tessier et al., 2007). In the subsequent steps, the main processing unit is the sub-image, except for the voting stage which integrates results coming from several sub-images.

2.2. Feature extraction

A machine vision system can extract many types of features from rocks that can be categorized in three groups: color, texture and morphology. Since our processing unit is the sub-image, we do not consider morphological features (rock shape and size) and, as in Tessier et al. (2007), in our work only color and textural features are considered.

In rock classification, color features have been widely used (Chatterjee et al., 2010a, 2010b; Lepisto et al., 2005; Singh and Rao, 2006; Tessier et al., 2007) since the natural coloration of a mineral constitutes an essential characteristic. Nevertheless, color similarities could exist between different minerals. The RGB space is perhaps the most popular image representation and has also been widely used in rock classification. Other representations are HSV, normalized RGB, and YCbCr. Each channel of the selected representation contains a very large amount of information depending on the size of the image and, therefore, several techniques have been used to extract and represent the color information. For example, Principal Component Analysis (PCA), histogram parameters, as well as Gabor filters have been used to represent color features. In this study we used PCA applied to the RGB representation to extract color features, although other color representations were also explored. Specifically, we adopted the multi-way PCA utilized by Tessier et al. (2007). The

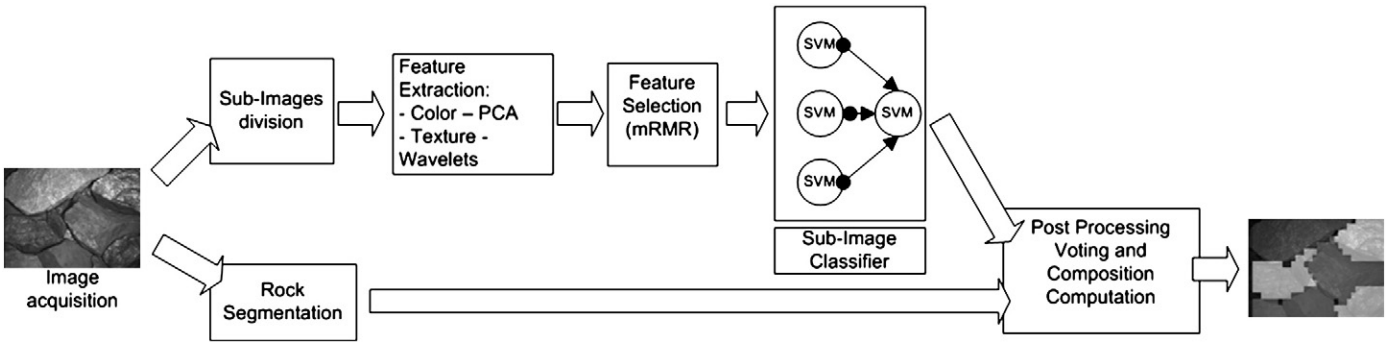

Fig. 1. Block diagram of the proposed method for rock composition estimation.

reader is referred to that study for further details. Kachanubal and Udomhunsakul (2008) also used PCA for color feature extraction.

Let I be one of the 512 sub-images reshaped into an $n*m\times 3$ matrix, with n and m, the width and height of the sub-image, respectively. I can be expressed in terms of the N loading vectors, p_k, and the N score vectors, t_k, as follows:

$$I = \sum_{k=1}^{N} t_k p_k + E, \tag{1}$$

where the matrix E contains the residuals. In Eq. (1) t_k is an $n*m$ column vector and p_k is three-dimensional. We considered the first two loading vectors as color descriptors and thus contributed with six color features for each sub-image.

Texture features account for spatial variations, i.e., information about the spatial arrangement of intensities in a selected region of an image. Texture is very important in rock classification since it has great influence on rock parameters such as penetrability (Hoseinie et al., 2009) and helps in understanding the conditions under which rock crystallizes (Singh et al., 2010). Some of the rock texture characteristics are mineral content, packing, grain size and shape, bonding structure, etc. Among the techniques used for texture analysis in digital images are the Fourier transform, the wavelet transform, Markov modeling, Gabor filtering, and the Haralick texture features, among others. In the present paper, we utilized the Wavelet Texture Analysis (WTA) approach since it has already been successfully used in rock classification (Tessier et al., 2007). Wavelet functions have also been used by Murtagh and Starck (2008) for texture feature extraction in rock classification.

The WTA is a multi-resolution signal analysis based on wavelet transform which is a two-dimensional discrete transform for images (Mallat, 1989). It performs low-pass (with the scaling function) and high-pass (with the wavelet function) filtering followed by decomposition to compute the dimension called detail which can be in any direction. The process can be viewed as a decomposition using a set of independent frequency channels with spatial orientation specificity (Mallat, 1989). We used the Daubechies wavelets with two levels of decomposition, although other wavelet families such as Morlet and Haar were also explored with similar results.

The texture feature vector was constructed with first and second order statistics of the detail (three directions), matrices using energy and Haralick features (Haralick, 1979), which have been used before for rock texture characterization (Chatterjee et al., 2010a, 2010b; Linek et al., 2007; Paclik et al., 2005; Singh and Rao, 2006). We used four Haralick features computed on the co-occurrence matrix $M(i,j)$ estimated as follows:

$$\text{Energy}: E = \sum_{i,j} M^2(i,j), \tag{2}$$

$$\text{Entropy}: S = \sum_{i,j} M(i,j)\log(M(i,j)), \tag{3}$$

$$\text{Contrast}: Con = \sum_{i,j} |i-j|^k M^l(i,j), \tag{4}$$

$$\text{Correlation}: Cor = \sum_{i,j} \frac{(i-\mu)(j-\mu)M(i,j)}{\sigma^2}. \tag{5}$$

We normalized the energy (Eq. (2)) with the max sum of the co-occurrence matrix. For the contrast (Eq. (4)) we set $k=2$ and $l=1$. In Eq. (5), the correlation, μ and σ represent the mean and the standard deviation, respectively. The co-occurrence matrix $M(i,j)$ counts the presence of pixel pairs (i,j) for a given displacement vector. For example, if the displacement vector is unitary and horizontal, then $M(i,j)$ specifies the number of times that the pixel with value i occurred horizontally adjacent to a pixel with value j. Thus, M is nxn with n the number of gray levels used to represent the image. We tested unitary displacements in four directions and used 16 levels for representation.

The final feature vector is the concatenation of color and texture features. We used 6 color descriptors as explained above. In the WTA we used two levels of decomposition leading to 6 detailed matrices that generate 30 descriptors: the energy of the 6 matrices plus 4 Haralick features for each of the computed co-occurrence matrices. Therefore, the length of the concatenated final vector was 36.

2.3. Feature selection

Starting from a large number of features extracted from input data, feature selection is the process of selecting a subset of relevant features which contain useful information for distinguishing one class from the others (Vinh et al., 2010). One of the main goals of feature selection is to represent the data in a lower dimensional space (Sun et al., 2002a). An additional benefit of feature selection is the reduction in computational time. In particular computational time is a key feature for image processing applications that require real-time performance (Perez et al.,2007). In particular, rock composition monitoring in mining applications requires real-time computation. The feature vector containing color and texture descriptors is reduced by means of feature selection. The idea is to find a subspace of $m<N$ features from the N-dimensional observation space that characterizes the data so that classification error is reduced. This subspace is difficult to find exhaustively because the total number of subspaces is 2^N and also m is not known in advance (Peng et al., 2005). We used a method based on mutual information to search this subspace: the minimal-redundancy-maximal-relevance (mRMR) (Peng et al., 2005).

Let MI be the mutual information between two random variables, X and Y, defined in terms of the probabilistic density functions $p(x)$, $p(y)$ of X and Y, respectively, and the joint probability density function $p(x,y)$, as follows (Estevez et al., 2009):

$$\text{MI}(x,y) = \iint p(x,y)\,\log\frac{p(x,y)}{p(x)p(y)}dxdy. \tag{6}$$

The mRMR relies on two constraints based on mutual information. First, a maximal relevance criterion is implemented to search features x_i with the largest mutual information $MI(x_i,c)$ with the target class c. This is accomplished by maximizing the following function:

$$D(S,c) = \frac{1}{|S|}\sum_{x_i\in S} MI(x_i,c). \tag{7}$$

However, class separation is not greatly affected if two or more features depend heavily on each other. Therefore, a second criterion is used to select mutually exclusive features by minimizing the following function:

$$R(S) = \frac{1}{|S|^2}\sum_{x_i,x_j\in S} MI\left(x_i,x_j\right). \tag{8}$$

2.4. Classifier

Once the feature vector has been reduced by means of the feature selection process, each vector x_s is assigned to one of three classes using a classifier. In a similar manner as in Tessier et al. (2007), we employed three SVMs coupled in cascade as a classifier. The SVM has become very popular within the machine learning community due to its great classification potential (Meyer et al., 2003). The SVM maps input vectors in a non-linear transformation to a high-dimensional space where a linear decision hyper-plane is constructed for class separation (Cortes and Vapnik, 1995). Although the SVM was originally

designed to solve a two-class problem, the extension for the separation of three classes is straightforward. In this study we coupled two layers of three-class SVMs in cascade, as shown in Fig. 1. The first layer consists of three SVMs where the input to each SVM is the reduced feature vector x_S, and the output is a scalar representing the predicted class. In the second layer only one SVM is used. The input to this classifier is a three-dimensional vector containing the predictions of the previous layer, and the output is the final prediction of the entire classification system.

2.5. Rock segmentation and voting process

Rock segmentation refers to the process of automatic separation of rocks or rock fragments within the image using digital image processing techniques. In this study, we use rock segmentation to identify blobs that belong to the same rock and therefore, sub-images that fall within each blob should have labels of the same class. The classification labels obtained for each of the sub-images are combined in a voting manner within each rock fragment or blob according to the segmentation. Each rock fragment is assigned to the class with the most votes. According to our literature review, this voting scheme has not been used before in rock segmentation. We proposed very recently a similar approach for biometric face recognition using Gabor jets where a weighted voting is used together with a threshold that allows the elimination of weak scores (Perez et al., 2011; Perez et al., 2010).

Several methods have been proposed for rock segmentation in the past few years, including those based on thresholding, region growing, region splitting and merging, and the approach based on abrupt changes in gray-level pixels (Wang, 2008). In the literature concerning the general problem of segmentation, the Watershed algorithm (Beucher and Lantuejoul, 1979) is highly relevant and has also been used in rock segmentation (Salinas et al., 2005). This non-parametric algorithm has the advantage that no threshold value is needed (Beucher and Lantuejoul, 1979). It is based on mathematical morphology and its conception comes from geography. Let us assume that the image border map is a topographic relief and that water falls in it. Water starts filling the gaps reaching a minimum height. Thus, the Watershed lines are the borders of the catchment basins that overlap, i.e., points of the relief where the water reaches the minimum height. Formally, the set of Watershed lines W can be defined as in Eq. (9)

$$W = \bigcup_{\lambda} S\left(Y_{\lambda} - \bigcup_{\mu<\lambda} W_{\mu}; X_{\lambda}\right), \tag{9}$$

where the sub-index indicates that the point (or set) has the specified height, so that the term $Y\lambda - \bigcup_{\mu<\lambda} W_{\mu}$ represents the sets of points belonging to only one catchment basin with height less than λ. The set $S(Y,X)$ is called the skeleton by zone of influence of Y with respect to X and includes the points of X at an infinite distance from Y or points equidistant from two different connected components.

The success of the Watershed segmentation relies on the election of appropriate 'seeds' before filling the catchment basins (Salinas et al., 2005), which can be determined manually. We implemented a novel scheme to automatically determine an appropriate set of seeds for the rock images. This seed creation algorithm seeks rock cores applying morphological operations, motivated by the fact that in an image of rock mixture, each rock center represents a candidate for a catchment basin in the Watershed algorithm. It starts with Gaussian low-pass filtering and histogram equalization. Then several morphological operations (Soille, 2003) are applied over the gray level image, including erosion, opening by dilatation, closing by reconstruction and regional maxima. It is worth noting that these morphological operations are extensions of the binary operations used widely in binary image processing. Other studies also use gray level morphological operations for rock segmentation (Chatterjee et al., 2010a, 2010b). Finally, resulting blobs are filtered by size, followed by a final block of morphological operations. Using these seeds generated with this algorithm, we tested the Watershed implementation available in the OpenCV library for machine vision. Fig. 2 shows an example of the Watershed seed initialization and rock boundary detection.

Once the border map is obtained, blobs are defined as regions within the image that fall within a closed loop. Then, a classification correction is applied on each blob assuming that all sub-images within the same blob are of the same class. A voting scheme is used in which all sub-images within the blob vote for the class they belong to and the blob class is the one with the most sub-image votes if the class with most votes is over a confidence threshold.

The process is repeated for all blobs. Finally, the estimated area composition of minerals in the image is computed using the corrected results for all sub-images. Fig. 3 shows an example of this voting process applied to an image of rocks from the database. Fig. 3(a) shows the original rocks in the image, Fig. 3(b) shows the results of the sub-image classification assigning one gray level to each of the three rock classes; gray level 1 for class 1, gray level 2 for class 2 and gray level 3 for class 3. Fig. 3(c) shows the results of using the boundary information from the Watershed segmentation to perform voting among all sub-images within a single blob. Fig. 3(d) shows the superposition of the final sub-image classification, after voting, and the original rock image. The voting method corrects some isolated misclassifications and thus increases the performance of the overall system. A second strategy was introduced to improve the accuracy of rock classification using the border map information. Results coming from sub-images with a high content of borders are assumed to barely contribute to estimation of mineral composition, because of both the

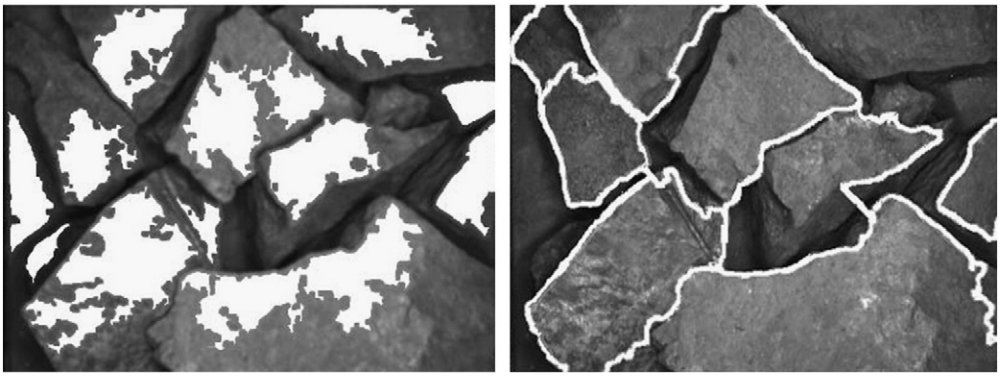

Fig. 2. Example of the proposed Watershed rock segmentation. On the left image the seeds initialization is shown and on the right image the final rock segmentation is shown.

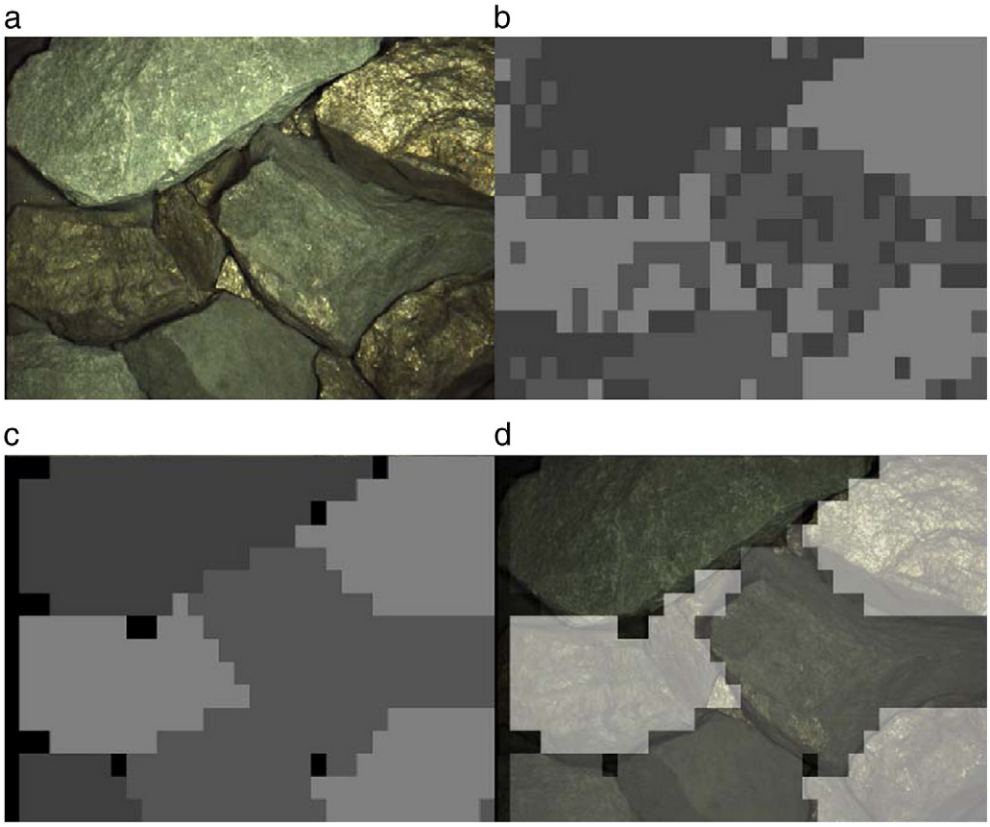

Fig. 3. Shows an example of the sub-image voting process applied on a rock image. (a) Shows original rocks in the image, (b) shows the results of the sub-image classification assigning one gray level to each of the three rock classes. (c) Shows the results of using the boundary information from the Watershed segmentation to perform voting among all sub-images within a single blob. (d) Shows the superposition of the final sub-image classification, after voting, and the original rock image.

absence of rocks and/or the mixture of several small rock fragments. Therefore, these sub-images are excluded from the final voting process.

2.6. Rock database

We tested our method on the rock database used by Tessier et al. (2007). This database was collected using a high resolution color camera mounted on a pilot plant with each digital image 1024 × 1376 pixels. Fig. 4 shows an example of captured rocks on a conveyor belt. The rock samples were extracted from Raglan's nickel mine in Quebec, Canada, and contain five different ore types: massive sulfide (MS), disseminated sulfide (DS), "net textured" (NT), gabbro (G), and peridotite (P). These minerals can be classified according to their grindability in three groups: soft (MS), medium (DS and NT), and hard (G and P), with increasing hardness and density and, importantly, a decreasing level of nickel content. An experienced mineralogist manually classified these minerals according to the visual appearance of rock surfaces (color and texture) and shapes (morphology) (Tessier et al., 2007). The main objective of the machine vision system is to correctly identify the composition of these three grindability classes within a sample of rock mixture.

Fig. 4. An example of rocks in an image from the database.

2.7. Performance measurement

In order to assess the performance of the proposed method quantitatively for on-line mineral composition estimation, we introduced two error measures that allow us to compare our results to those of the ground truth, i.e., the real composition of minerals in terms of weight. Thus, area estimations must first be converted into weight estimations. This was achieved by simply multiplying areas by mineral densities, and thus assuming constant rock load thickness (Tessier et al., 2007).

Let $r_{i,t}$ be the real weight proportion of rocks belonging to class i in time t, $w_{i,t}$ the estimated weight proportions using the machine vision system, and N the total number of images. Then the error associated to each class e_i can be computed as follows:

$$e_i = \sqrt{\frac{1}{\mathrm{N}}\sum_{t=0}^{\mathrm{N}}\left(r_{i,t}-w_{i,t}\right)^2}. \tag{10}$$

The error e_i, also known as Root Mean Square Error (RMSE), accounts for temporal variations in the load or sampled mixtures of rocks and it is useful for a general framework of rock weight proportion estimation. In order to obtain a single error measure, the Euclidean norm of the error per class is computed as

$$Er = \sqrt{\sum_{i=1}^{3} e_i^2}. \tag{11}$$

2.8. Experiments

We performed experiments to test the proposed rock classification method and compare our results to those previously published. We had 1098 available images from Tessier et al. (2007) database which were composed of 530 pure (265 dry and 265 wet rock images) and 568 mix rock images (284 dry and 284 wet rock images).

We used the 530 pure rock partition (265 dry and 265 wet rock images) as the training and validation dataset. This dataset corresponds to experiments 11 and 14 to 17 in Tessier et al. (2007).

We used the 568 mix rock images as the test dataset (284 dry and 284 wet rock images). This dataset corresponds to experiments 1 to 10 and 12 and 13 in Tessier et al. (2007).

Thus, each image was partitioned in 512 sub-images as described in the Methods.

From the training dataset a total of 50 dry rock images and 50 wet rock images were built with pure sub-images (512) eliminating background and rock edges. Therefore, a total of 51,200 pure sub-images of 64×43 pixels were available for training and validation. The whole training set was divided in 10 subsets, each one composed by one image of each rock type. Therefore, each subset contains one class of soft rock images, two classes of medium and two classes of hard rock images. Using the 100 images, a 10 fold cross-validation approach was used in order to choose best parameters for the SVM classifier. Therefore, 10 different SVM parameters were determined for testing that was performed on the 568 mix rock partition.

As in Tessier et al. (2007), and using the same training set of 100 images, a second experiment was performed training and testing only with dry rock images. In the same manner a third experiment was performed training and testing only with wet rock images. In experiments two and three training was performed with 10 dry or wet rock images and a 5 fold cross-validation approach was used in order to choose best parameters for the SVM classifier. Therefore 5 different SVM parameters were determined and testing was performed in the test dataset of 568 mix images (284 dry and 284 wet rock images).

The proposed method requires the choice of two thresholds, one to eliminate sub-images with high content of borders and a second one called confidence threshold used in the voting process. The choice was made using the training and validation partition of 530 pure images. A set of threshold was tested ranging from 0.1 to 0.9. The border threshold of 0.4 and the confidence threshold of 0.6 were chosen. Using the same validation dataset 14 features were selected from the 36 possible features using mRMR.

3. Results and discussion

In order to compare our results to those reported by Tessier et al. (2007), we extracted the data from graphs presented in Fig. 15 in Tessier et al. (2007) using the xyExtract software. Thus, for each point in the graph we determine the error between the predicted composition by the model and the ground truth. From this error we determine the RMSE.

Table 1 shows the RMSE for the test dataset of 568 mix rock images (284 dry and 284 wet rock images) where the model was trained with dry and wet rocks. The first column shows the simulation number from 1 to 10. The second column shows the results for each of the 10 trained SVM models using only the sub-image classification to determine the composition. This result includes the feature selection using mRMR. On the third column of Table 1, the RMSE is shown when voting is added to the sub-image classification using information from manual rock segmentation (segmentation ground truth). The fourth column shows the RMSE using voting among the sub-images that fall within the blob given by the automatic Watershed segmentation. The first row shows the results from Tessier et al. (2007).

Table 1
RMSE measured on the Mix testing dataset including dry and wet rock images. The second column shows the RMSE for each of the 10 trained SVM models using only the sub-image classification. The third column shows the RMSE with voting using manual rock segmentation. The fourth column shows the RMSE using voting for the automatic watershed segmentation. The first row on the fifth column shows the results from Tessier et al. (2007).

	Mix test			
	Sub-image	Voting: manual segmentation	Voting: watershed segmentation	Tessier et al. (2007)
Tessier et al. (2007)				44
1	34	29	30	
2	33	30	30	
3	34	29	30	
4	34	31	32	
5	34	30	31	
6	38	32	34	
7	35	31	32	
8	34	31	31	
9	33	29	30	
10	34	30	31	
Average	34	30	31	
Std dev	1.4	1.0	1.3	

Comparing RMSE averages and standard deviations it is possible to determine that the error results including voting (30 ± 1.0 for manual segmentation and 31 ± 1.3 for Watershed segmentation) are lower with statistical significance (t-test, $p<0.0001$) with respect to direct (34 ± 1.4) sub-image classification. The RMSE decreased 8.8% by using our proposed voting method with the automatic Watershed segmentation with respect to direct sub-image classification. The RMSE decreased 29.5% relative to previously published results with the same database using mix rock images.

Table 2 shows the RMSE for the test dataset of 284 dry mix rock images where the model was trained with dry rocks from the training set. The first column shows the simulation number from 1 to 5. The second column shows the results for each of the 5 trained SVM models using only the sub-image classification to determine the composition. This result includes the feature selection using mRMR. On the third column of Table 2, the RMSE is shown when voting is added to the sub-image classification using information from manual rock segmentation (segmentation ground truth). The fourth column shows the RMSE using voting among the sub-images that fall within the blob given by the automatic Watershed segmentation. The first row shows the results from Tessier et al. (2007).

In the case of training and testing with only dry rock images it is possible to compare the RMSE averages and standard deviations 25 ± 0.8 for manual segmentation and 27 ± 1.1 for Watershed segmentation are lower with statistical significance (t-test, $p<0.0001$) with respect to

Table 2
RMSE measured on the Mix testing dataset including only dry rock images. The second column shows the RMSE for each of the 5 trained SVM models using only the sub-image classification. The third column shows the RMSE with voting using manual rock segmentation. The fourth column shows the RMSE using voting for the automatic watershed segmentation. The first row on the fifth column shows the results from Tessier et al. (2007).

	Mix test			
	Sub-image	Voting: manual segmentation	Voting: watershed segmentation	Tessier et al. (2007)
Tessier et al. (2007)				33
1	28	24	25	
2	30	26	27	
3	34	26	28	
4	31	25	27	
5	30	25	26	
Average	31	25	27	
Std dev	2.2	0.8	1.1	

Table 3
RMSE measured on the Mix testing dataset including only wet rock images. The second column shows the RMSE for each of the 5 trained SVM models using only the sub-image classification. The third column shows the RMSE with voting using manual rock segmentation. The fourth column shows the RMSE using voting for the automatic watershed segmentation. The first row on the fifth column shows the results from Tessier et al. (2007).

	Mix test			
	Sub-image	Voting: manual segmentation	Voting: watershed segmentation	Tessier et al. (2007)
Tessier et al. (2007)				54
1	32	27	28	
2	32	28	28	
3	32	28	28	
4	33	28	29	
5	31	27	27	
Average	32	28	28	
Std dev	0.7	0.5	0.7	

direct (31 ± 2.2) sub-image classification. The RMSE decreased 12.9% by using our proposed voting method with the automatic Watershed segmentation with respect to direct sub-image classification. The most important result is that the RMSE decreased 18.2% relative to previously published results with the same database for dry rock classification.

Table 3 shows the RMSE for the test dataset of 284 wet mix rock images where the model was trained with wet rocks from the training set. The first column shows the simulation number from 1 to 5. The second column shows the results for each of the 5 trained SVM models using only the sub-image classification to determine the composition. This result includes the feature selection using mRMR. On the third column of Table 3, the RMSE is shown when voting is added to the sub-image classification using information from manual rock segmentation (segmentation ground truth). The fourth column shows the RMSE using voting among the sub-images that fall within the blob given by the automatic Watershed segmentation. The first row shows the results from Tessier et al. (2007).

In the case of training and testing with only wet rock images it is possible to compare the RMSE averages and standard deviations 28 ± 0.5 for manual segmentation and 28 ± 0.7 for Watershed segmentation are lower with statistical significance (t-test, $p<0.0001$) with respect to direct (32 ± 0.7) sub-image classification. The RMSE decreased 12.5% by using our proposed voting method with the automatic Watershed segmentation with respect to using direct sub-image classification. The RMSE decreased 48.1% relative to previously published results with the same database of only wet rocks.

Fig. 5 and Fig. 6 show the estimation of rock composition per class using manual and Watershed segmentation, respectively. Both figures show in solid line the target, black squares our proposed method and gray circles the previously published results (Tessier et al., 2007).

The result improvements by our proposed method without voting over previous results can be explained by our feature selection. Our approach, based on MI uses all statistical information about the

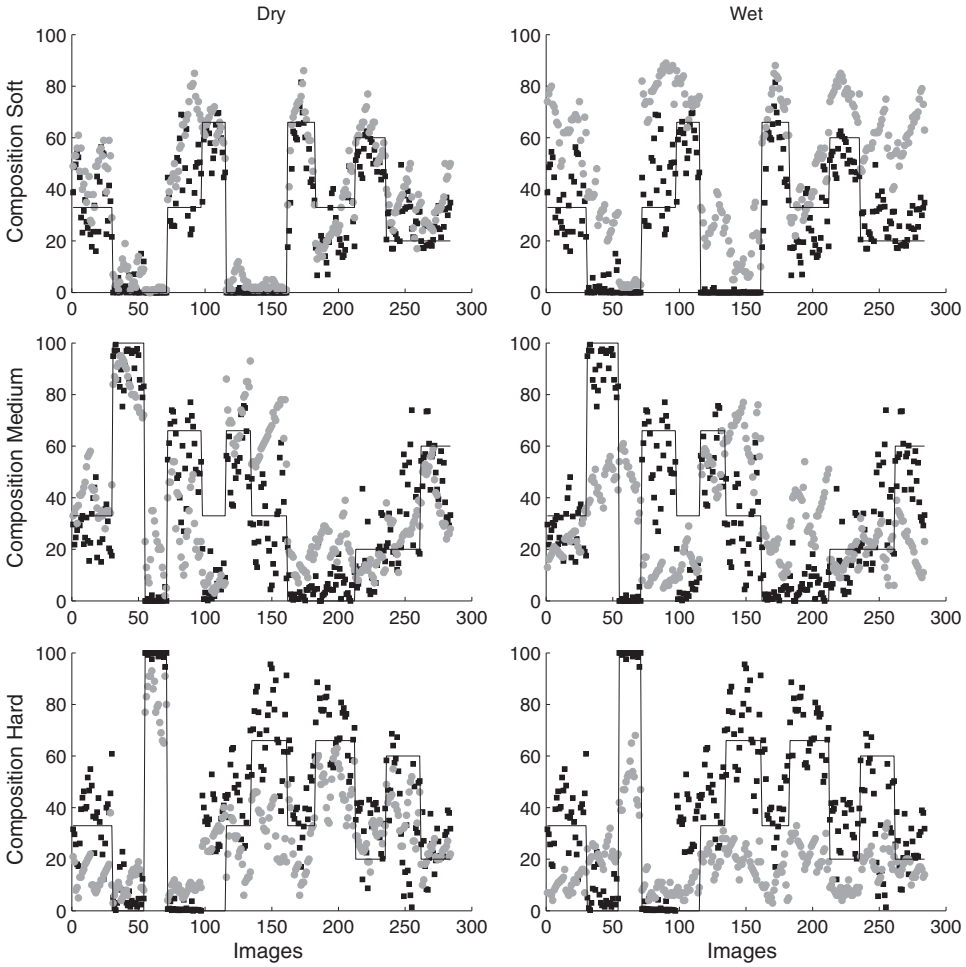

Fig. 5. Shows the estimation of rock composition per class using manual segmentation. The figure shows in solid line the target, black squares our proposed method and gray circles the previously published results (Tessier et al., 2007).

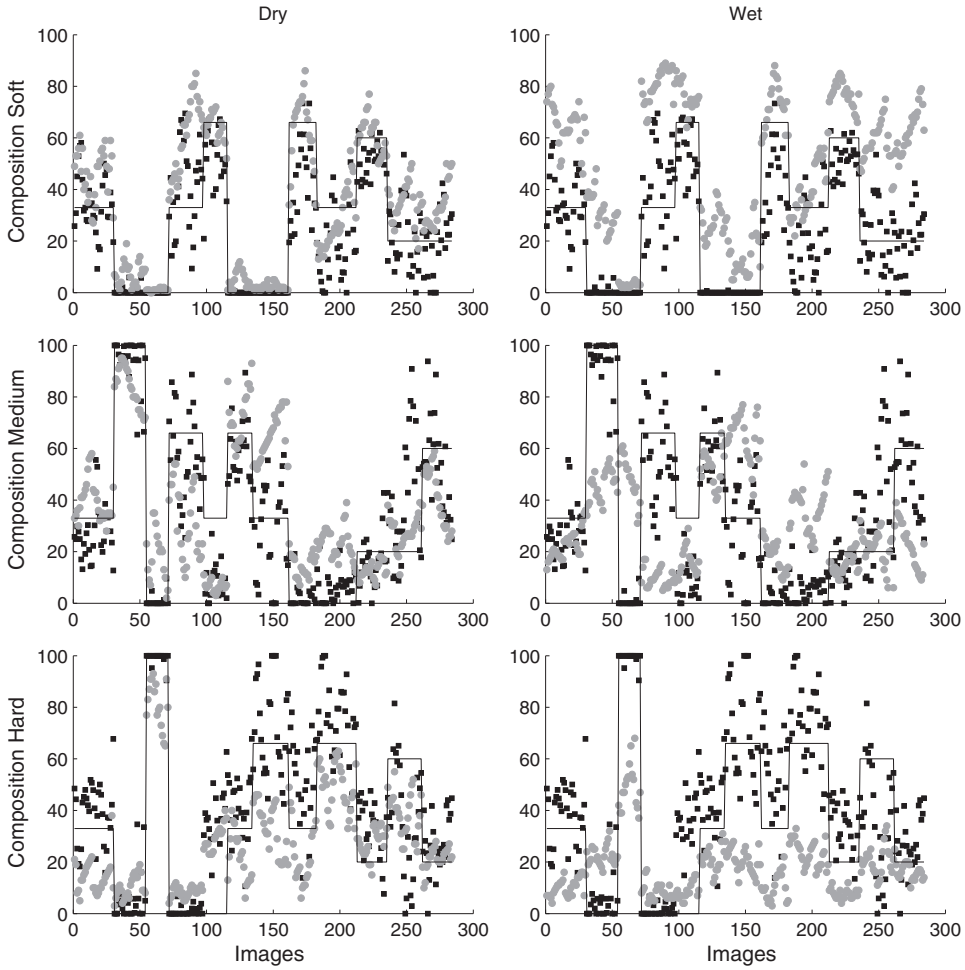

Fig. 6. Shows the estimation of rock composition per class using Watershed segmentation. The figure shows in solid line the target, black squares our proposed method and gray circles the previously published results (Tessier et al., 2007).

probability distribution of the input features. Another method, such as Partial Least Squares (PLS) used in previous research (Tessier et al., 2007) is a linear regression and therefore some information can be lost when projecting to a three dimensional space.

Another source of result improvements is the proposed voting process among sub-images within each blob. The information about boundary for different rocks can be extracted by image analysis methodology and could be improved by using range imaging in the future.

We believe that in a conveyor belt application where rock samples might be captured over long periods of time and with a sampling rate determined by the camera frame rate, temporal information could be very useful to improve classification just like in face recognition. For example, it has been shown that by integrating results obtained from different frames, a more accurate prediction can be achieved (Ekenel et al., 2010). The integration method can be as simple as a voting scheme, although other strategies such as Markov hidden models or probabilistic frameworks can be used. Future research in on-line ore classification/sorting systems could tackle this issue.

4. Conclusion

A new rock classification method based on image processing was presented in this study. Significant improvement was shown by introducing a post-processing voting stage that combines rock segmentation with classification correction to enhance the estimation of rock types present in the mixture. The proposed method could be used for automatic on-line rock classification and sorting which in turn could help in optimizing, for instance, the throughput of mills within a mine. Error estimations were also presented for quantitative assessment of the machine vision system. The method reached results significantly better than those previously reported on a database of rock images captured from a pilot plant with nickel loads, although it could be used to classify other minerals.

Acknowledgments

We would like to thank Prof. Carl Duchesne from Université Laval, Canada, for providing us the rock database used in Tessier et al. (2007). This research has been funded by the Advanced Mining Technology Center (AMTC), Universidad de Chile, and by FONDEF project D08I1060 from Conicyt, Chile.

References

Al-Batah, M.S., Isa, N.A.M., Zamli, K.Z., Sani, Z.M., Azizli, K.A., 2009. A novel aggregate classification technique using moment invariants and cascaded multilayered perceptron network. International Journal of Mineral Processing 92 (1–2), 92–102.

Aldrich, C., Marais, C., Shean, B.J., Cilliers, J.J., 2010. Online monitoring and control of froth flotation systems with machine vision: a review. International Journal of Mineral Processing 96 (1–4), 1–13.

Al-Thyabat, S., Miles, N.J., Koh, T.S., 2007. Estimation of the size distribution of particles moving on a conveyor belt. Minerals Engineering 20 (1), 72–83.

Beucher, S., Lantuejoul, C., 1979. Use of watersheds in contour detection. International Workshop on Image Processing: Real-time Edge and Motion Detection/Estimation, Rennés, France, pp. 17–21.

Casali, A., Gonzalez, G., Vallebuona, G., Perez, C., Vargas, R., 2001. Grindability soft-sensors based on lithological composition and on-line measurements. Minerals Engineering 14 (7), 689–700.

Chatterjee, S., Bandopadhyay, S., Machuca, D., 2010a. Ore grade prediction using a genetic algorithm and clustering based ensemble neural network model. Mathematical Geosciences 42 (3), 309–326.
Chatterjee, S., Bhattacherjee, A., Samanta, B., Pal, S.K., 2010b. Image-based quality monitoring system of limestone ore grades. Computers in Industry 16 (5), 391–408.
Cortes, C., Vapnik, V., 1995. Support-vector networks. Machine Learning 20 (3), 273–297.
Donskoi, E., Suthers, S.P., Campbell, J.J., Raynlyn, T., 2008. Modelling and optimization of hydrocyclone for iron ore fines beneficiation — using optical image analysis and iron ore texture classification. International Journal of Mineral Processing 87 (3–4), 106–119.
Ekenel, H.K., Stallkamp, J., Stiefelhagen, R., 2010. A video-based door monitoring system using local appearance-based face models. Computer Vision and Image Understanding 114 (5), 596–608.
Estevez, P.A., Tesmer, M., Perez, C.A., Zurada, J.A., 2009. Normalized mutual information feature selection. IEEE Transactions on Neural Networks 20 (2), 189–201.
Goncalves, L.B., Leta, F.R., de Valente, S.C., 2009. Macroscopic rock texture image classification using an hierarchical neuro-fuzzy system. Systems, Signals and Image Processing, 2009. IWSSIP 2009. 16th International Conference on, pp. 1–5.
Guyot, O., Monredon, T., LaRosa, D., Broussaud, A., 2004. VisioRock, an integrated vision technology for advanced control of comminution circuits. Minerals Engineering 17 (11–12), 1227–1235.
Haralick, R.M., 1979. Statistical and structural approaches to texture. Proceedings of the IEEE 67 (5), 786–804.
Hoseinie, S.H., Ataei, M., Osanloo, M., 2009. A new classification system for evaluating rock penetrability. International Journal of Rock Mechanics and Mining Sciences 46 (8), 1329–1340.
Hunter, G.C., McDermott, C., Miles, N.J., Singh, A., Scoble, M.J., 1990. A review of image analysis techniques for measuring blast fragmentation. Mining Science and Technology 11 (1), 19–36.
Kachanubal, T., Udomhunsakul, S., 2008. Rock textures classification based on textural and spectral features. International Journal of Computational Intelligence 4, 240–246.
Koh, T.K., Miles, N.J., Morgan, S.P., Hayes-Gill, B.R., 2009. Improving particle size measurement using multi-flash imaging. Minerals Engineering 22 (6), 537–543.
Lepisto, L., Kunttu, I., Visa, A., 2005. Rock image classification using color features in Gabor space. Journal of Electronic Imaging 14 (4).
Linek, M., Jungmann, M., Berlage, T., Pechnig, R., Clauser, C., 2007. Rock classification based on resistivity patterns in electrical borehole wall images. Journal of Geophysics and Engineering 4 (2), 171–183.
Mallat, S.G., 1989. A theory for multiresolution signal decomposition: the wavelet representation. IEEE Transactions on Pattern Analysis and Machine Intelligence 11 (7), 674–693.
Meyer, D., Leisch, F., Hornik, K., 2003. The support vector machine under test. Neurocomputing 55 (1–2), 169–186.
Murtagh, F., Starck, J.L., 2008. Wavelet and curvelet moments for image classification: application to aggregate mixture grading. Pattern Recognition Letters 29 (10), 1557–1564.
Oestreich, J.M., Tolley, W.K., Rice, D.A., 1995. The development of a color sensor system to measure mineral compositions. Minerals Engineering 8 (1–2), 31–39.
Paclik, P., Verzakov, S., Duin, R.P.W., 2005. Improving the maximum-likelihood co-occurrence classifier: a study on classification of inhomogeneous rock images. Proceedings Image Analysis, 3540, pp. 998–1008.
Peng, H.C., Long, F.H., Ding, C., 2005. Feature selection based on mutual information: criteria of max-dependency, max-relevance, and min-redundancy. IEEE Transactions on Pattern Analysis and Machine Intelligence 27 (8), 1226–1238.
Perez, C., Casali, A., Gonzalez, G., Vallebuona, G., Vargas, R., 1999. Lithological composition sensor based on digital image feature extraction, genetic selection of features and neural classification, ICIIS'99. Proc. 1999 IEEE International Conference on Information Intelligence and Systems, Bethesda, MD, Oct.31-Nov.3, pp. 236–241.
Perez, C.A., Lazcano, V.A., Estevez, P.A., 2007. Real-time iris detection on coronal-axis-rotated faces. IEEE Transactions on Systems, Man, and Cybernetics-Part C 37 (5), 971–978.
Perez, C.A., Aravena, C.M., Vallejos, J.I., Estevez, P.A., Held, C.M., 2010. Face and iris localization using templates designed by particle swarm optimization. Pattern Recognition Letters 31 (9), 857–868.
Perez, C.A., Cament, L.A., Castillo, L.E., 2011. Methodological improvement on local Gabor face recognition based on feature selection and enhanced Borda count. Pattern Recognition 44 (4), 951–963.
Petersen, K.R.P., Aldrich, C., Van Deventer, J.S.J., 1998. Analysis of ore particles based on textural pattern recognition. Minerals Engineering 11 (10), 959–977.
Salinas, R.A., Raff, U., Farfan, C., 2005. Automated estimation of rock fragment distributions using computer vision and its application in mining. IEE Proceedings: Vision, Image and Signal Processing 152 (1), 1–8.
Singh, V., Rao, S., 2006. Application of image processing in mineral industry: a case study of ferruginous manganese ores. Mineral Processing and Extractive Metallurgy 115 (3), 155–160.
Singh, N., Singh, T.N., Tiwary, A., Sarkar, K.M., 2010. Textural identification of basaltic rock mass using image processing and neural network. Computational Geosciences 14 (2), 301–310.
Soille, P., 2003. Morphological Image Analysis: Principles and Applications, 2nd Ed. Springer, Berlin, New York.
Sun, Z., Bebis, G., Yuan, X., Louis, S.J., 2002. Genetic feature subset selection for gender classification: a comparison study. Proc. Sixth IEEE Workshop Applications of Computer Vision (WACV), pp. 165–170.
Tessier, J., Duchesne, C., Bartolacci, G., 2007. A machine vision approach to on-line estimation of run-of-mine ore composition on conveyor belts. Minerals Engineering 20 (12), 1129–1144.
Thurley, M.J., Ng, K.C., 2008. Identification and sizing of the entirely visible rocks from a 3D surface data segmentation of laboratory rock piles. Computer Vision and Image Understanding 111 (2), 170–178.
Vinh, L.T., Thang, N.D., Lee, Y.K., 2010. An improved maximum relevance and minimum redundancy feature selection algorithm based on normalized mutual information. International Symposium on Applications and the Internet (SAINT), 10th IEEE/IPSJ, Seoul, Korea, pp. 395–398.
Wang, W., 2008. Rock particle image segmentation and systems in pattern recognition. In: Yin, P.-Y. (Ed.), Pattern Recognition Techniques, Technology and Applications. InTech, Croatia, pp. 197–226.